Surface wave ray tracing and azimuthal anisotropy: a generalized spherical harmonic approach

Lapo Boschi[1] and John H. Woodhouse[2]

[1]*E.T.H. Zürich, Institute of Geophysics, Hönggerberg HPP, CH-8093 Zürich, Switzerland. E-mail: boschi@tomo.ig.erdw.ethz.ch*
[2]*University of Oxford, Department of Earth Sciences, Parks Road, Oxford, OX1 3PR, UK*

SUMMARY
We explain in detail how azimuthally anisotropic maps of surface wave phase velocity can be parametrized in terms of generalized spherical harmonic functions, and why this approach is preferable to others; most importantly, generalized spherical harmonics are the only basis functions adequate to describe a tensor field everywhere on the unit sphere, including the poles of the reference frame. We introduce here a new algorithm, designed specifically for the generalized harmonic parametrization, to trace surface wave ray paths in the presence of laterally varying azimuthal anisotropy. We describe the algorithm, and prove its reliability in view of future applications.

Key words: global seismology, ray theory, ray tracing, seismic anisotropy, spherical harmonics, surface waves.

1 INTRODUCTION

In the context of wave propagation, we call 'anisotropic' a medium where the speed of a wave at each point depends on its direction of propagation. In the Earth, we speak of 'azimuthal anisotropy' when the wave speed changes with the azimuth of the seismic ray, with respect to a fixed direction (usually the north or the east). Smith & Dahlen (1973, 1975) first wrote a theoretical relation, valid in a half-space medium, between slight perturbations δc in the phase velocity c of Love and Rayleigh waves, and the azimuth ζ of their direction of propagation,

$$\frac{\delta c(\mathbf{r}, \zeta)}{c} = \epsilon_0(\mathbf{r}) + \epsilon_1(\mathbf{r})\cos(2\zeta) + \epsilon_2(\mathbf{r})\sin(2\zeta)$$
$$+ \epsilon_3(\mathbf{r})\cos(4\zeta) + \epsilon_4(\mathbf{r})\sin(4\zeta), \tag{1}$$

where $\mathbf{r}$ is a two-vector denoting position on the half-space surface, and the values of $\epsilon_i (i = 0, \ldots, 4)$ naturally change also as functions of surface wave frequency ω.

Eq. (1) has been used to set up tomographic inverse problems, based upon the ray theory approximation, to derive global maps of the azimuthal anisotropy of Rayleigh and Love waves (Tanimoto & Anderson 1984, 1985; Montagner & Tanimoto 1990; Laske & Masters 1998; Ekström 2001; Trampert & Woodhouse 2003). The effect of azimuthal anisotropy on surface wave propagation was assumed to be small, and anisotropic maps were derived as small perturbations to isotropic reference models. This way, the problem of ray tracing through anisotropic media was avoided. Only few authors (Tanimoto 1987; Mochizuki 1990; Larson *et al.* 1998) extended Woodhouse & Wong's (1986) work in surface wave ray tracing, to account for the effects of slowly laterally varying azimuthal anisotropy on JWKB surface wave ray paths.

From Larson *et al.*'s (1998) article, one gathers that their implementation of ray-tracing equations is entirely numerical, or

rests on the interpretation of eq. (1) as a purely scalar relationship, with a pixel, or spline parametrization of anisotropic maps. Trampert & Woodhouse (2003), in agreement with the earlier works of Mochizuki (1986, 1993), suggest that generalized spherical harmonics (e.g. Phinney & Burridge 1973; Dahlen & Tromp 1998, appendix C) provide a more adequate parametrization; in fact, physical observables like the direction of fastest propagation, which should have a regular behaviour throughout the globe, are likely to become singular at the poles of the reference frame, when ϵ_i are described over grids of pixels or splines, or as combinations of non-generalized ('scalar') harmonics. The problem is avoided when a generalized spherical harmonic parametrization is chosen (Fig. 1). (Note that Larson *et al.* (1998, eq. 2.41) do make use of generalized spherical harmonics, but in an entirely different sense.)

We describe here a new surface wave ray tracing algorithm, valid in the presence of azimuthal anisotropy, based on a generalized spherical harmonic expansion of anisotropic phase velocity maps. Our procedure is the most natural extension to the case of azimuthal anisotropy of what has been done, with scalar spherical harmonic parametrizations, for isotropic surface wave propagation; accordingly, anisotropic maps expressed as combinations of generalized spherical harmonics can be more easily rotated than pixel/spline maps, to have the source–receiver great circle coincide with the equator (simplifying the implementation of ray-tracing equations), analytical results are available for path integrals and model derivatives with respect to position, and the map resolution is independent of location and of the reference frame.

2 THE GENERALIZED HARMONIC PARAMETRIZATION

We shall describe here in more detail the treatment of Trampert & Woodhouse (2003, Section 2).
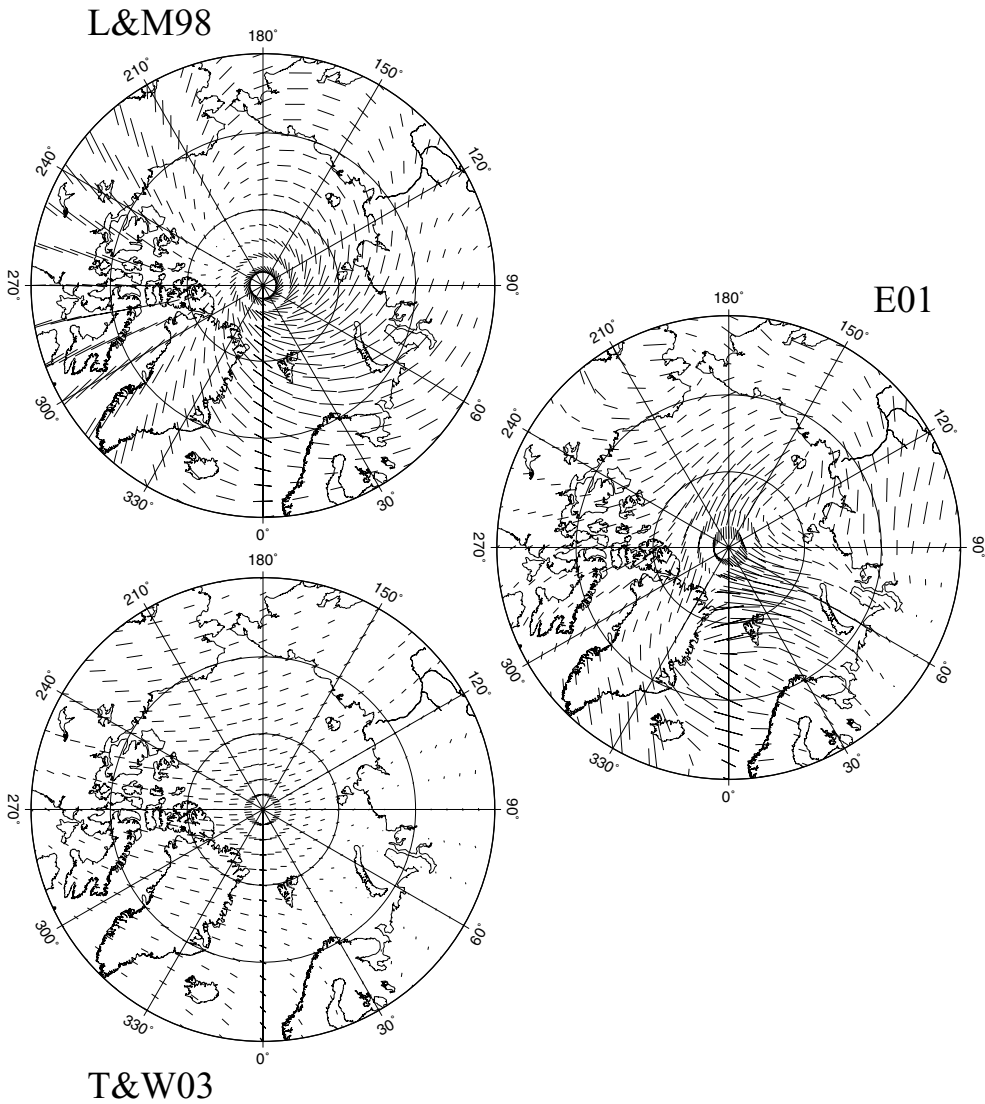
GJI Seismology

Figure 1. 2ζ direction of fastest propagation, $1/2 \operatorname{atan}(\epsilon_2/\epsilon_1)$, shown with a stereographic projection around the North Pole, as mapped by Laske & Masters (1998) (L& M98) from 80 s Rayleigh wave surface wave observations, and Ekström (2001) (E01) and Trampert & Woodhouse (2003) (T& W03) from 100 s Rayleigh wave observations. The length of each segment is proportional to the amplitude of anisotropy.

Because generalized spherical harmonics are designed to describe tensor, rather than scalar fields, we shall first rewrite eq. (1) in tensorial form. Let us start by introducing a 2×2 tensor $\boldsymbol{\tau}(\theta, \phi)$, with components

$$\tau_{\theta\theta} = -\tau_{\phi\phi} = \epsilon_1, \tag{2}$$

$$\tau_{\theta\phi} = \tau_{\phi\theta} = -\epsilon_2, \tag{3}$$

and a $2 \times 2 \times 2 \times 2$ tensor $\boldsymbol{\sigma}(\theta, \phi)$, with

$$\sigma_{\theta\theta\theta\theta} = \sigma_{\phi\phi\phi\phi} = \epsilon_3, \tag{4}$$

$$\sigma_{\theta\theta\phi\phi} = -\epsilon_3, \tag{5}$$

$$\sigma_{\theta\theta\theta\phi} = -\sigma_{\phi\phi\phi\theta} = \epsilon_4 \tag{6}$$

(Trampert & Woodhouse 2003); the remaining entries of $\boldsymbol{\sigma}$ coincide with those whose indexes are a permutation of theirs, for example, $\sigma_{\theta\theta\theta\phi} = \sigma_{\theta\theta\phi\theta} = \sigma_{\theta\phi\theta\theta} = \sigma_{\phi\theta\theta\theta}$, and so forth. Note that both $\boldsymbol{\tau}$

and $\boldsymbol{\sigma}$ are thus completely symmetric and trace-free. Denoting $\boldsymbol{\nu} = (-\sin(\zeta), \cos(\zeta))$, eq. (1) can be written

$$\frac{\delta c(\theta, \phi, \zeta)}{c} = \epsilon_0(\theta, \phi) + \nu_i \nu_j \tau_{ij}(\theta, \phi) + \nu_i \nu_j \nu_k \nu_l \sigma_{ijkl}(\theta, \phi), \tag{7}$$

where summation over repeated indices is implicit. In tensor notation,

$$\frac{\delta c(\theta, \phi, \zeta)}{c} = \epsilon_0(\theta, \phi) + \boldsymbol{\nu} \cdot \boldsymbol{\tau}(\theta, \phi) \cdot \boldsymbol{\nu} + \boldsymbol{\nu}\boldsymbol{\nu} : \boldsymbol{\sigma}(\theta, \phi) : \boldsymbol{\nu}\boldsymbol{\nu}. \tag{8}$$

Again, dependence on the surface wave frequency ω is understood.

In Section 4, we shall require the azimuth to be measured counter-clockwise from east. Eq. (1), however, holds independently of the azimuth convention, although in general to a different definition of ζ will correspond different numerical values of $\epsilon_i (i = 0, \ldots, 4)$; it should be noted that, had the ray path azimuth in eq. (1) been defined with respect to the north (e.g. Trampert & Woodhouse 2003) rather than east, $\boldsymbol{\tau}$ and $\boldsymbol{\sigma}$ would remain unchanged, provided that cosine and sine be swapped in the definition of $\boldsymbol{\nu}$; eqs (7) and (8) would then also hold in their present form.

If the tensors τ and σ, and the vector ν are rotated according to the rotation rule for tensors, eqs (7) and (8) will keep their form in the rotated system, with no need to find ζ from ζ' (azimuth in the rotated system) at each Runge-Kutta step.

Just like scalar functions on a sphere are most conveniently expressed as linear combinations of scalar spherical harmonics, vectors and higher- order tensors should be written as combinations of generalized spherical harmonics. In particular, it is useful to expand the 'contravariant' components of a tensor of order q in terms of generalized spherical harmonics $Y_{lm}^N(\theta, \phi)$, as defined in Appendix A below, with N depending on q and on the tensor component indexes (e.g. Phinney & Burridge 1973; Dahlen & Tromp 1998, Appendix C; Trampert & Woodhouse 2003); this way, the generalized spherical harmonic coefficients of the rotated tensor can be simply found by an ordinary matrix multiplication between its coefficients in the initial reference frame, and a rotation matrix whose entries, quite interestingly, are simply related to the values of generalized Legendre functions (e.g. Dahlen & Tromp, Sections C.8.2 and C.8.6).

Let us denote τ^{++}, τ^{-+}, τ^{+-}, τ^{--} the contravariant components of τ. They are related to its θ, ϕ components through eq. (2.4) of Phinney & Burridge (1973), simplified after accounting for the lack of radial dependence of τ here,

$$\tau^{++} = \tau_{\theta\theta} - i\tau_{\theta\phi}, \tag{9}$$

$$\tau^{--} = \tau_{\theta\theta} + i\tau_{\theta\phi}, \tag{10}$$

and $\tau^{+-} = \tau^{-+} = 0$. The latter equation further simplifies the treatment that follows, with respect to that of Phinney & Burridge (1973), as it implies that only generalized spherical harmonics with $N = \pm 2$ are needed.

From eqs (9) and (10) the relations

$$\tau_{\theta\theta} = \frac{1}{2}(\tau^{--} + \tau^{++}), \tag{11}$$

$$\tau_{\theta\phi} = \frac{1}{2i}(\tau^{--} - \tau^{++}) \tag{12}$$

follow. For eq. (7) to have physical meaning, the θ, ϕ components of τ have to be real; this, together with eqs (11) and (12), implies

$$\tau^{++} = \tau^{--*}, \tag{13}$$

with the superscript $*$ denoting complex conjugation. Generalized spherical harmonic coefficients τ_{lm}^{++} and τ_{lm}^{--} of the contravariant components of the second-order tensor τ are defined

$$\tau^{++}(\theta, \phi) = \sum_{l=0}^{\infty} \sum_{m=-l}^{l} \tau_{lm}^{++} Y_{lm}^2(\theta, \phi), \tag{14}$$

$$\tau^{--}(\theta, \phi) = \sum_{l=0}^{\infty} \sum_{m=-l}^{l} \tau_{lm}^{--} Y_{lm}^{-2}(\theta, \phi). \tag{15}$$

Substituting eqs (14) and (15) into (13),

$$\sum_{l=0}^{\infty} \sum_{m=-l}^{l} \tau_{lm}^{++} Y_{lm}^2(\theta, \phi) = \sum_{l=0}^{\infty} \sum_{m=-l}^{l} \tau_{lm}^{--*} Y_{lm}^{-2*}(\theta, \phi), \tag{16}$$

and making use of the relation

$$Y_{lm}^{-2*} = (-1)^m Y_{l-m}^2 \tag{17}$$

[e.g. Phinney & Burridge 1973, Appendix A; Dahlen & Tromp 1998, eqs (C.118)] and of the orthogonality of generalized spherical harmonics, we prove the symmetry relation

$$\tau_{lm}^{++} = (-1)^m \tau_{l-m}^{--*}. \tag{18}$$

The number of coefficients necessary to express a real second-order tensor as a combination of generalized spherical harmonics is half that needed for a complex second-order tensor.

Now, after substituting eq. (9) on the left-hand side of eq. (14) [equivalently, we could plug eq. (10) into the left-hand side of eq. (15)],

$$\tau_{\theta\theta} - i\tau_{\theta\phi} = \sum_{l=0}^{\infty} \sum_{m=-l}^{l} \tau_{lm}^{++} Y_{lm}^2(\theta, \phi), \tag{19}$$

and equating the real and imaginary parts separately, we find

$$\tau_{\theta\theta} = \sum_{l=0}^{\infty} \sum_{m=-l}^{l} \left(\text{Re}(\tau_{lm}^{++})\text{Re}(Y_{lm}^2) - \text{Im}(\tau_{lm}^{++})\text{Im}(Y_{lm}^2) \right), \tag{20}$$

$$\tau_{\theta\phi} = \sum_{l=0}^{\infty} \sum_{m=-l}^{l} \left(- \text{Im}(\tau_{lm}^{++})\text{Re}(Y_{lm}^2) - \text{Re}(\tau_{lm}^{++})\text{Im}(Y_{lm}^2) \right), \tag{21}$$

where we have denoted $\text{Re}(z)$ and $\text{Im}(z)$, respectively, the real and imaginary parts of any complex number z. Eqs (20) and (21) imply that only generalized spherical harmonics with $N = +2$ need to be computed. As it is customary with scalar spherical harmonics in problems involving real functions (e.g. Dahlen & Tromp 1998), in software implementations it is preferable to treat $\text{Re}(Y_{lm}^2)$ and $\text{Im}(Y_{lm}^2)$ as separate real functions, and store $\text{Re}(\tau_{lm}^{++})$ and $\text{Im}(\tau_{lm}^{++})$ as independent real arrays. Denoted L the chosen maximum value of l where, in practical applications, we interrupt the harmonic series, we find that $2(L + 1)^2$ real coefficients ($\text{Re}(\tau_{lm}^{++})$, $\text{Im}(\tau_{lm}^{++})$) are sufficient to identify both $\tau_{\theta\theta}$ and $\tau_{\theta\phi}$. This number is reduced to $2(L + 1)^2 - 8$ when we take into account that $Y_{lm}^2 = 0$ for $l < 2$. Note that $2(L + 1)^2 - 8 = (2L + 6)(L - 1)$ (Trampert & Woodhouse 2003).

A similar treatment (eqs 9–21) holds for the σ term of eqs (7) and (8), and we shall omit it here for brevity. Because $\delta c/c$ is real, we find that only coefficients $\text{Re}(\sigma_{lm}^{++++})$ and $\text{Im}(\sigma_{lm}^{++++})$ of the Y_{lm}^4 harmonics are needed to represent the '4ζ' anisotropic effect. Since $Y_{lm}^4 = 0$ for $l < 4$, this number reduces to $2(L + 1)^2 - 32 = (2L + 10)(L - 3)$ (Trampert & Woodhouse 2003).

3 OTHER PARAMETRIZATIONS

While the images of Trampert & Woodhouse (2003) have been derived directly as combinations of generalized spherical harmonics [eqs (20) and (21), and analogous expansions for $\sigma_{\theta\theta\theta\theta}$, $\sigma_{\theta\theta\theta\phi}$], other authors have employed different parametrizations. Laske & Masters (1998), for example, write ϵ_1 and ϵ_2 as independent linear combinations of scalar, real spherical harmonics (and neglect ϵ_3, ϵ_4 in their tomographic inversion); Ekström (2001) prefers spherical splines (see also Becker *et al.* 2003).

Our preference for the generalized spherical harmonic parametrization is not a matter of subjective choice, but rests on theoretical considerations: the direction of fastest propagation ζ_{fast}, that is the value of ζ for which, at a given location **r**, $\delta c(\mathbf{r}, \zeta)/c$ is maximum, depends simultaneously on all $\epsilon_i(i = 1, \ldots, 4)$. Separate expansions of each ϵ_i, which can only extend up to a finite harmonic degree, implicitly require each ϵ_i to be relatively smooth, or well behaved throughout the globe, but do not grant that a physical observable like ζ_{fast} be globally well behaved at all: far from the poles of the reference frame, the smoothness of each ϵ_i is a sufficient condition for ζ_{fast} to be smooth; but near the poles ζ_{fast} might become singular as a result of each ϵ_i being smooth. (Likewise, the θ- and ϕ-components of a vector might each vary slowly near a pole,

and the vector itself be consequently undefined at the same pole.) The parametrization described here, with a tensorial expansion of τ and σ in terms of generalized harmonics, is a way of avoiding the problem altogether.

To illustrate this, we show in Fig. 1 maps of ζ_{fast} around the North Pole, derived by the authors mentioned above, and associated with Rayleigh waves at periods between 80 and 100 s. In all plots of Fig. 1 ϵ_3 and ϵ_4 are approximated with zero; the resulting quantity is usually referred to as '2ζ fast azimuth'. By equating to zero the

derivative of $\epsilon_1(\mathbf{r}) \cos(2\zeta) + \epsilon_2(\mathbf{r}) \sin(2\zeta)$ with respect to ζ, we find

$$\zeta_{\text{fast}} = \frac{1}{2} \text{atan} \left(\frac{\epsilon_2}{\epsilon_1} \right). \tag{22}$$

Laske & Masters' (1998) map is clearly singular at the North Pole (although very smooth if looked at in a cylindrical equatorial projection); Ekström's (2001) ζ_{fast} is better behaved, owing to an *ad hoc* design of the spline grid (Ekström, personal communication, 2005);
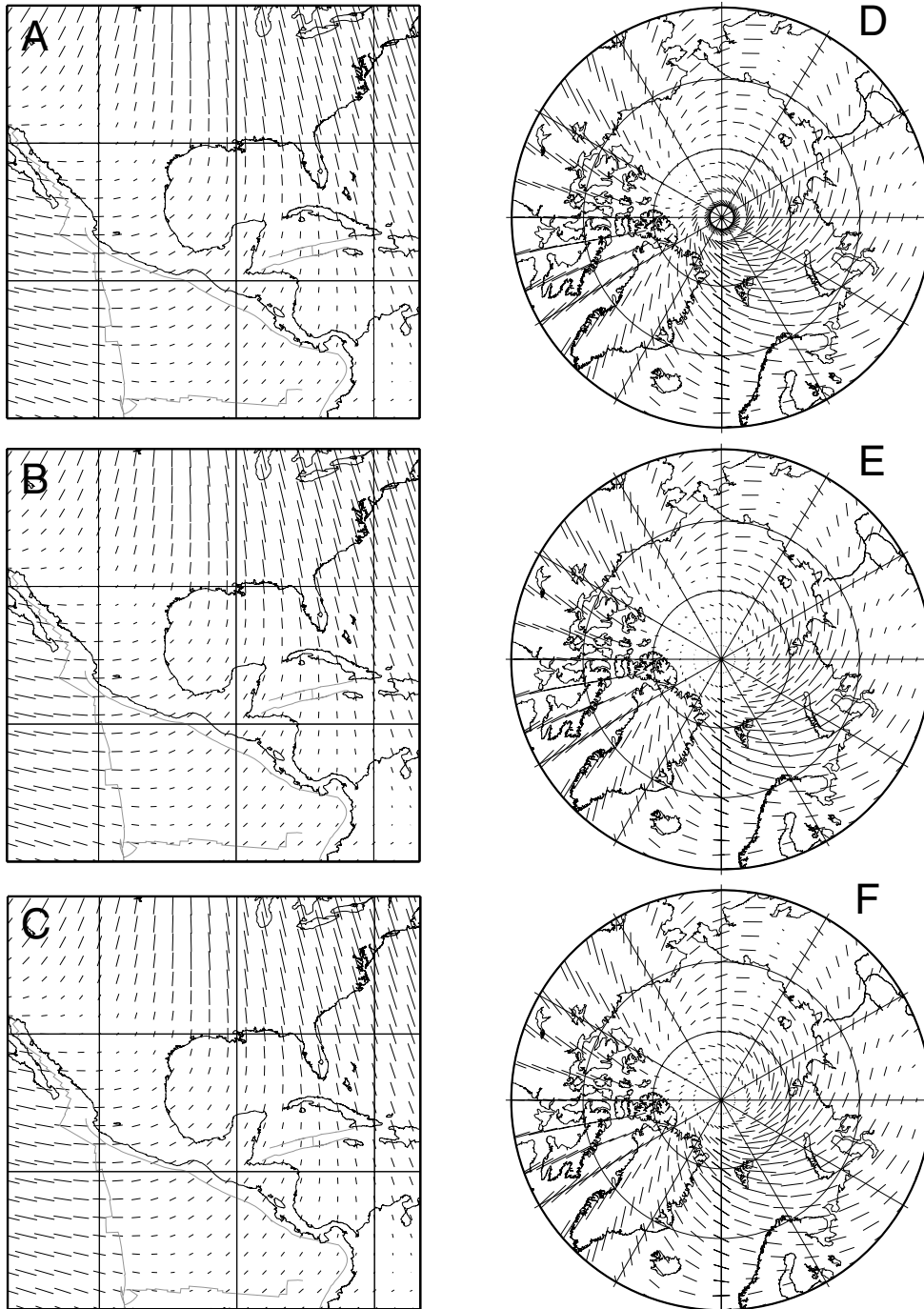

Figure 2. (a) 2ζ direction of fastest propagation in a region of relatively high anisotropy not far from the equator, from Laske & Masters (1998); (b) the same image, described as a sum over generalized spherical harmonics, up to degree 20; (c) same as (b), up to degree 29; (d), (e) and (f) same as (a), (b) and (c), but only the region of the same maps surrounding the North Pole is now shown, in a stereographic projection centred on the pole.

only Trampert & Woodhouse's (2003) image is entirely smooth at the pole.

The images of Fig. 1 were plotted based on each author's original parametrization. It is not difficult, however, to find the generalized harmonic expansion associated to each map. Anisotropic maps must first be evaluated at each node of a regular grid that covers the entire globe, the spacing between gridpoints being only limited by available computational memory and speed. At the ith gridpoint θ_i, ϕ_i we rewrite eqs (20) and (21),

$$
\begin{aligned}
\epsilon_1(\theta_i, \phi_i) = \sum_{l=0}^{L} \sum_{m=-l}^{l} & \left(\mathrm{Re}\left(\tau_{lm}^{++}\right) \mathrm{Re}\left(Y_{lm}^2(\theta_i, \phi_i)\right) \right. \\
& \left. - \mathrm{Im}\left(\tau_{lm}^{++}\right) \mathrm{Im}\left(Y_{lm}^2(\theta_i, \phi_i)\right) \right),
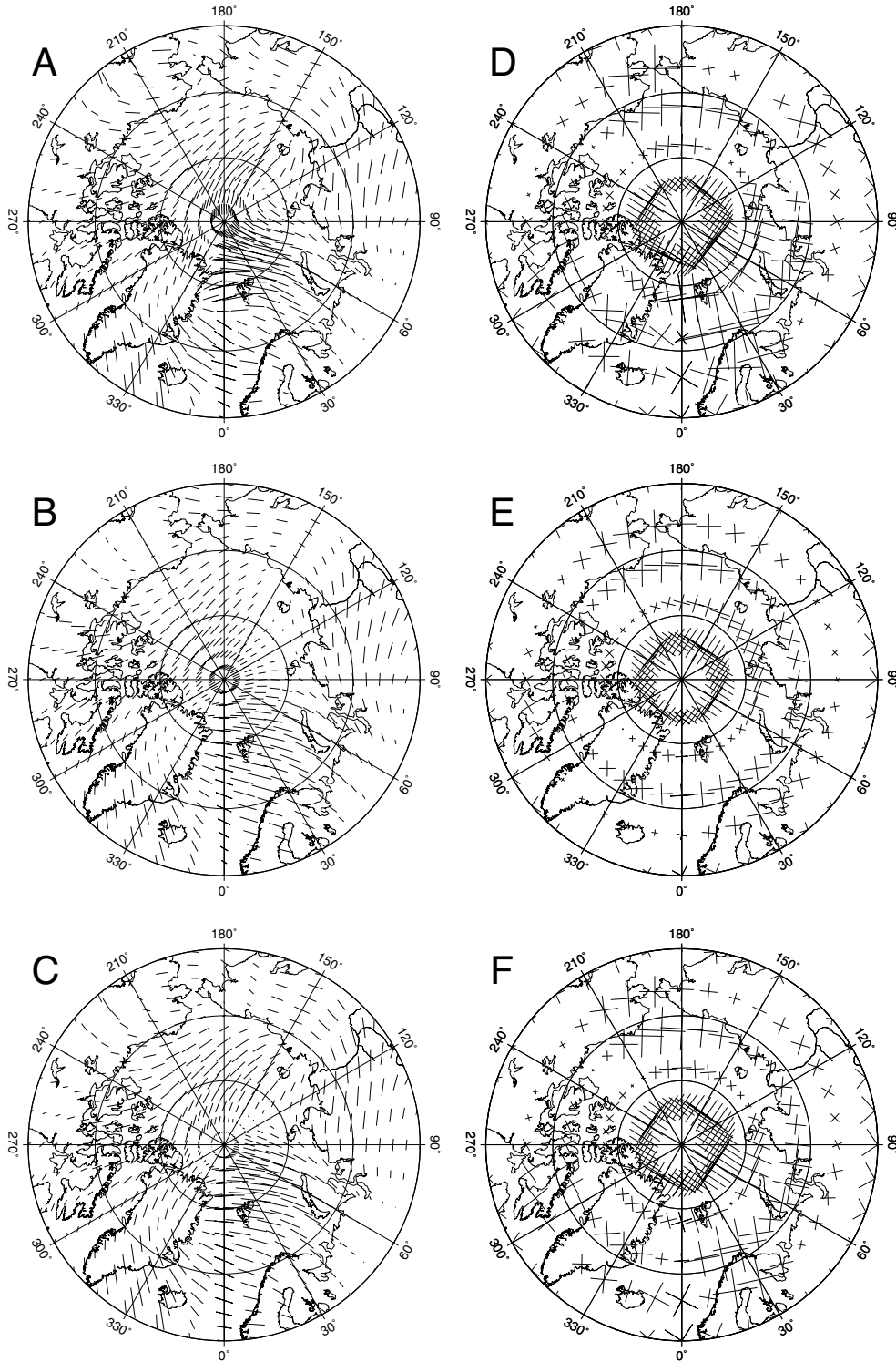\end{aligned} \tag{23}
$$

Figure 3. (a) 2ζ direction of fastest propagation around the North Pole, from Ekström (2001); (b) the same image, described as a sum over generalized spherical harmonics, up to degree 20; (c) same as (b), up to degree 29; (d), (e) and (f) are the same as (a), (b) and (c), respectively, but the 4ζ fast directions are shown.

$$\epsilon_2(\theta_i, \phi_i) = \sum_{l=0}^{L} \sum_{m=-l}^{l} \left(\text{Im}(\tau_{lm}^{++}) \text{Re}(Y_{lm}^2(\theta_i, \phi_i)) \right.$$
$$\left. + \text{Re}(\tau_{lm}^{++}) \text{Im}(Y_{lm}^2(\theta_i, \phi_i)) \right). \tag{24}$$

Each gridpoint thus identifies two rows of a matrix **B** whose entries coincide with the known values $\text{Re}(Y_{lm}^2(\theta_i, \phi_i))$, $\text{Im}(Y_{lm}^2(\theta_i, \phi_i))$ at all l, m (a one to one relation between the column index of **B** and the couple l, m is established). We then perform a least-squares fit to find the set of coefficients $\text{Re}(\tau_{lm}^{++})$, $\text{Im}(\tau_{lm}^{++})$ that best-fit ϵ_1 and ϵ_2, implementing the least squares formula via Cholesky factorization of $\mathbf{B}^T \cdot \mathbf{B}$ (e.g. Press *et al.* 1992, Chapters 2 and 15; Trefethen & Bau 1997, Lecture 11). It is remarkable that the problem turns out to be unstable unless ϵ_1 and ϵ_2 are fit simultaneously.

Naturally, we find generalized spherical harmonic coefficients of ϵ_3 and ϵ_4 by an analogous procedure, involving harmonics Y_{lm}^4.

The top panels of Fig. 2 show the 2ζ direction of fastest propagation, according to Laske & Masters' (1998), for 80 s Rayleigh waves; the middle panels are obtained after finding the generalized harmonic coefficients of the same maps, with the procedure outlined above, up to maximum degree $L = 20$; the bottom panels illustrate the result of extending the harmonic expansion to $L = 29$. Near the equator (left panels) all maps coincide regardless of the value of L: an expected result, since Laske & Masters' (1998) original parametrization only involved harmonics with $l \leq 12$. The right

panels of Fig. 2, on the other hand, prove the inadequacy of a scalar harmonic parametrization of tensorial quantities in the vicinity of a pole; not even the degree-29 expansion is sufficient to reproduce the image's ill behaviour in the vicinity of the pole: there, Laske & Masters' (1998) separate parametrization of ϵ_1 and ϵ_2 causes ζ_{fast} to become undefined.

Fig. 3 suggests that Ekström (2001) spline parametrization at least limits the problem in question; the $L = 29$ generalized harmonic expansion does not reproduce entirely well Ekström (2001) original map of the 2ζ fast direction (compare Figs 3a and c), but one must consider that Ekström (2001) map has a significant high-l component also elsewhere in the globe (Becker *et al.* 2003). Ekström's (2001) method will be described in full detail in an article that is currently in preparation (Ekströom, personal communication), and we postpone further discussion until after its publication.

4 RAY TRACING

Larson *et al.* (1998, eqs 3.15 and 3.16) have derived for the ray-tracing equations the simple form (consistent with the results of Woodhouse & Wong 1986)

$$\frac{d\theta}{d\phi} = -\frac{\sin(\theta)(\tan(\zeta) + \partial_\zeta \ln c)}{1 - \tan(\zeta)\partial_\zeta \ln c}, \tag{25}$$
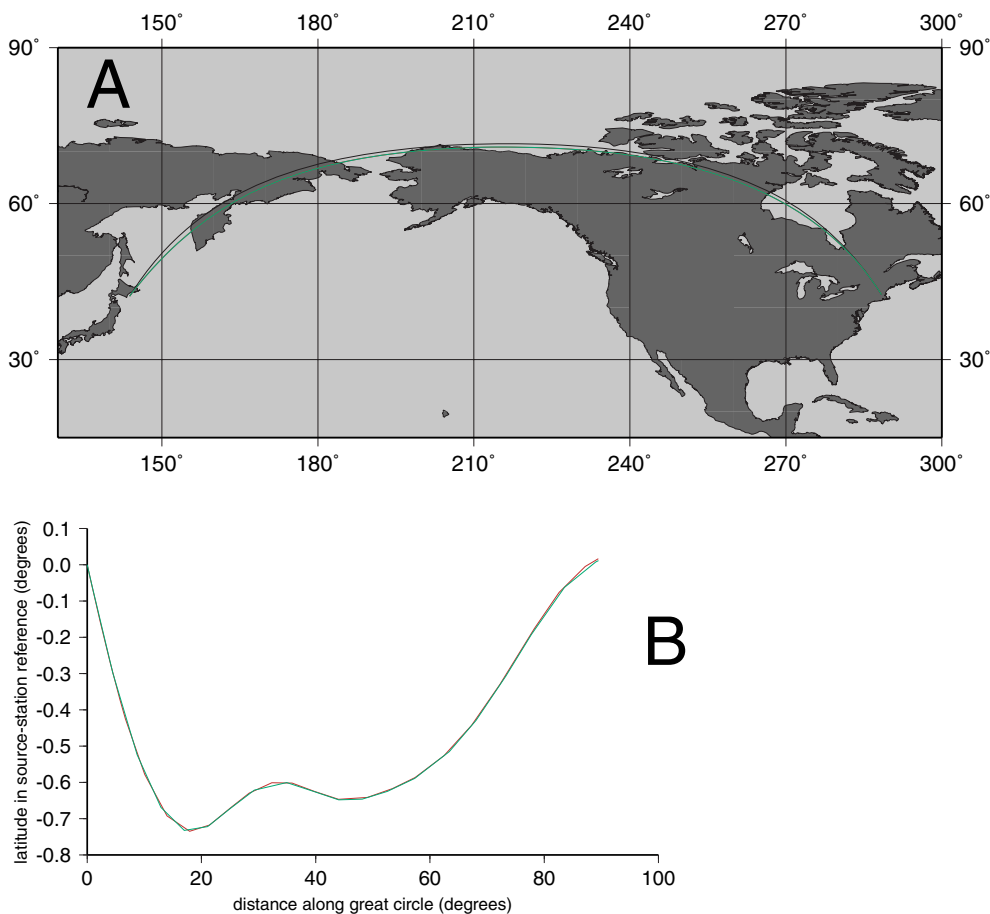

Figure 4. 100 s Rayleigh wave ray paths for an arbitrarily chosen source–receiver geometry (Hokkaido to HRV), traced by our algorithm in Trampert & Woodhouse's (2003) model. The isotropic, 2ζ and 4ζ terms were all accounted for. Plot A includes the great circle (black curve) connecting source and receiver, and the ray paths traced in the geographic (green curve) and rotated (red curve) reference frame. In this projection, no differences between the two ray paths can be observed, and the red curve is entirely hidden under the green one. In plot B, the same ray paths are plotted in the rotated reference frame, whose equator is identified by source and receiver, to emphasize discrepancies. Still, the two curves are practically coincident.

$$\frac{d\zeta}{d\phi} = \frac{\sin(\theta)\partial_\theta + \tan(\zeta)\partial_\phi \ln c - \cos(\theta)}{1 - \tan(\zeta)\partial_\zeta \ln c}, \qquad (26)$$

where θ denotes colatitude, ϕ longitude and ζ the ray path azimuth measured counter-clockwise from east.

Eqs (25) and (26) must be integrated numerically to find the ray path $\theta(\phi)$, $\zeta(\phi)$. Although they are valid in any reference frame, their numerical integration is only possible so long as θ is a single-valued function of ϕ; it is thus convenient to integrate them in a reference frame where both source and receiver are located on the equator. (For a ray-tracing algorithm to work regardless of the chosen reference frame, at least three ray-tracing equations have to be integrated simultaneously.)

We can see the integration of eqs (25) and (26) as a two-point boundary value problem (e.g. Press *et al.* 1992, Chapter 17) with ϕ as the independent parameter, and with the boundary condition $\theta = 0$ to be satisfied at source and receiver; we use here the fifth-order Cash-Karp Runge-Kutta method (Press *et al.* 1992, Chapter 16) to integrate from source to receiver, and, since the initial azimuth $\zeta(0)$ is unknown, we repeat the integration for a set of closely spaced values of $\zeta(0)$, until the one satisfying the requirement that $\theta = 0$ at the receiver is found. (We speak of 'multipathing' when more than one value of $\zeta(0)$ satisfy the boundary conditions.) The search for $\zeta(0)$ can be sped up, for example, through the shooting method (Press *et al.* 1992, Chapter 17).

The value of c in the rotated system is most efficiently derived by finding, before starting to integrate eqs (25) and (26), the generalized spherical harmonic coefficients of $\epsilon_i (i = 1, \ldots, 4)$ in the rotated frame; this is achieved with a simple dot multiplication between the corresponding non-rotated coefficient vectors and a rotation operator (Section 2 and Dahlen & Tromp 1998, Section C.8.6). The value of c at any location along the ray path is then found, at each step of the numerical integration of eqs (25) and (26), by a sum over generalized spherical harmonics in the rotated frame.

The issues of speed and accuracy in the computation of generalized harmonics are addressed in Appendix A below.

5 VALIDATION

We could not benchmark our algorithm by comparison with some established implementation of surface wave anisotropic ray theory, because no public-domain software currently exists for this purpose. We have devised a self-consistency test that is highly unlikely to prove successful unless the code is entirely error-free. The ray tracing eqs (25) and (26) are valid in any reference frame. Their numerical integration is also possible in any reference frame, so long as the function $\theta(\phi)$ that identifies the ray path remains single valued, which is the case for predominantly east–west ray paths, and so long as (θ, ϕ) is sufficiently far from the poles, where, in a non-rotated frame, the definition of ζ becomes ambiguous.

Given any eligible source-station couple, we can integrate eqs (25) and (26) both in the rotated and (after modifying the code slightly) geographical reference frames, and compare the results, as illustrated, for example, in Fig. 4, for the case of a 100 s surface wave travelling, in Trampert & Woodhouse's (2003) map, between the Hokkaido region in Japan and HRV station in Massachusetts; in Fig. 4(b) ray paths derived from the two approaches are compared in the rotated reference, and only a latitudinal band less than one degree away from the source-station great circle is shown, to emphasize discrepancies. Minor differences between the two curves result from differences in the Runge-Kutta stepsizes, which are independently determined according to the Cash-Karp Runge-Kutta method, and
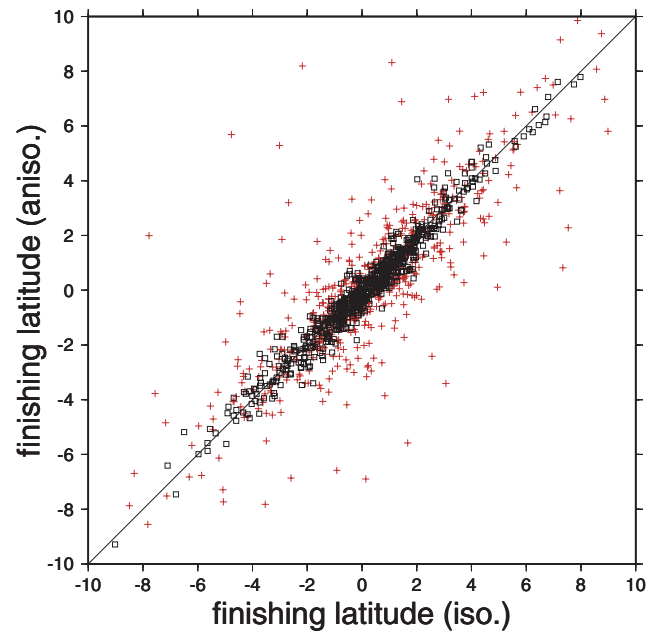

Figure 5. Finishing latitude (in degrees) of ray paths calculated in Ekström's (2001) (red crosses) and Trampert & Woodhouse's (2003) (black squares) 100 s Rayleigh wave propagation models, with (*y*-axis) versus without (*x*-axis) azimuthal anisotropy, from a set of randomly generated source-station couples.

change during integration (Press *et al.* 1992); otherwise, the two ray paths can be considered coincident.

We have successfully repeated this exercise for a number of randomly chosen source-station couples, with latitude of both source and station $\leq 45°$, and source-station azimuth between $50°$ and $130°$, or $230°$ and $310°$ (i.e. predominantly east–west).

6 CONCLUSIONS

Generalized spherical harmonics provide the most natural parametrization of azimuthally anisotropic maps of surface wave phase velocity. Only in a generalized spherical harmonic description can the direction of fastest propagation be adequately represented throughout the globe, and discrete (pixel, splines) or scalar spherical harmonic parametrizations are likely to lead to non-physical singularities near the poles of the reference frame (Figs 1 and 3).

The generalized spherical harmonic parametrization is not less practical than discrete (pixel, splines) ones; coefficients of anisotropic maps in a rotated reference frame are found through a simple matrix multiplication of the coefficient vector; the θ and ϕ derivatives of the harmonics are known analytically; the resolution (the highest spatial frequency of lateral heterogeneities that can be described by a set of basis functions) does not change laterally, which is not the case for pixels or splines, and which might have a non-negligible effect on tomographic applications (Trampert & Woodhouse 2003).

We have implemented and validated a new surface wave ray-tracing algorithm, designed for generalized spherical harmonic parametrizations, and we have shown how any surface wave map can be converted to our format. This completes the work of Trampert & Woodhouse (2003), who applied the generalized spherical harmonic parametrization to tomographic mapping of anisotropic surface wave velocity anomalies.
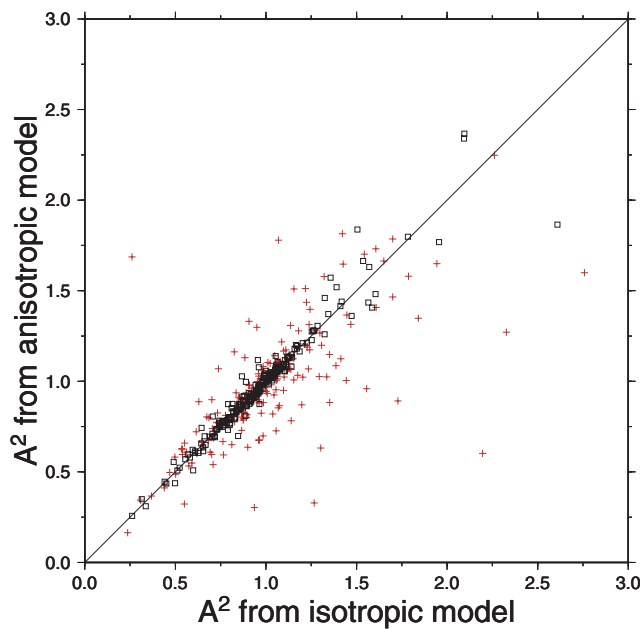
Figure 6. Squared amplitude anomaly with respect to a spherically symmetric earth model, derived with versus without azimuthal anisotropy, from both Ekström's (2001) (red crosses) and Trampert & Woodhouse's (2003) (black squares) models, for the same source-station couples as Fig. 5.

Two preliminary applications of our algorithm are illustrated in Figs 5 and 6.

Following Tape (2003), we employ the 'finishing latitude' (i.e. the latitude $90° - \theta(\Delta)$ of a path's endpoint in the rotated frame) of a ray, as a simple measure of the cumulative effect of the heterogeneities (isotropic/anisotropic) it encounters. We have traced rays with and without taking account of anisotropy, and plotted in Fig. 5 their finishing latitude found from azimuthally anisotropic maps, against that found from the isotropic component of the model only; we have repeated this exercise for both Ekström's (2001) and Trampert & Woodhouse's (2003) 100 s Rayleigh wave velocity maps. The stronger azimuthal anisotropy mapped by Ekström (2001) results in systematically larger path anomalies, at least for Rayleigh waves at 100 s period, with an effect comparable to that of purely isotropic anomalies.

For the same set of source-station couples, we have computed the squared ratio A^2 (given by eq. 41 of Woodhouse & Wong 1986, where a square root is missing) of 100 s Rayleigh wave amplitude from our ray-tracing algorithm, versus amplitude of the same waves in PREM; we have repeated this exercise in the presence and in the absence of azimuthal anisotropy, and, for each source-station couple, plotted in Fig. 6 the result of the former calculation against that of the latter. In agreement with Fig. 5, the anisotropy maps of Ekström (2001) have a stronger effect on surface wave amplitude.

Discrepancies between published maps of azimuthal anisotropy, and their relation to observables like arrival angles, phase and amplitude anomalies of surface waves, deserve further investigation, subject of our future work.

ACKNOWLEDGMENTS

REFERENCES

Becker, T.W., Kellogg, J.B., Ekström, G. & O'Connell, R.J., 2003. Comparison of azimuthal seismic anisotropy from surface waves and finite-strain from global mantle-circulation models, *Geophys. J. Int.,* **155,** 696–714.

Dahlen, F.A. & Tromp, J., 1998. *Theoretical Global Seismology*, Princeton University Press, New Jersey, USA.

Edmonds, A.R., 1960. *Angular Momentum in Quantum Mechanics*, Princeton University Press, New Jersey, USA.

Ekström, G., 2001. Mapping azimuthal anisotropy of intermediate-period surface waves (abstract), *EOS, Trans. Am. geophys. Un.,* **82**(47), S51E-06.

Larson, E.W.F., Tromp, J. & Ekström, G., 1998. Effects of slight anisotropy on surface waves, *Geophys. J. Int.,* **132,** 654–666.

Laske, G. & Masters, G., 1998. Surface wave polarization data and global anisotropic structure, *Geophys. J. Int.,* **132,** 508–520.

Masters, G. & Richards-Dinger, K., 1998. On the efficient calculation of ordinary and generalized spherical harmonics, *Geophys. J. Int.,* **135,** 307–309.

Mochizuki, E., 1986. The free oscillations of an anisotropic and heterogeneous Earth, *Geophys. J. R. astr. Soc.,* **86,** 167–176.

Mochizuki, E., 1990. Simple formulae for path and amplitude anomalies of anisotropic surface waves, *Geophys. J. Int.,* **102,** 263–264.

Mochizuki, E., 1993. Spherical harmonic analysis in terms of line integral, *Phys. Earth planet. Inter.,* **76,** 97–101.

Montagner, J.-P. & Tanimoto, T., 1990. Global anisotropy in the upper mantle inferred from the regionalization of phase velocities, *J. geophys. Res.,* **95,** 4797–4819.

Phinney, R.A. & Burridge, R., 1973. Representation of the elastic-gravitational excitation of a spherical Earth model by generalized spherical harmonics, *Geophys. J. R. astr. Soc.,* **34,** 451–487.

Press, W.H., Teukolsky, S.A., Vetterling, W.T. & Flannery, B.P., 1992. *Numerical Recipes in FORTRAN*, Cambridge University Press, UK.

Smith, M.L. & Dahlen, F.A., 1973. The azimuthal dependence of Love and Rayleigh wave propagation in a slightly anisotropic medium, *J. geophys. Res.,* **78,** 3321–3333.

Smith, M.L. & Dahlen, F.A., 1975. Correction to 'The azimuthal dependence of Love and Rayleigh wave propagation in a slightly anisotropic medium', *J. geophys. Res.,* **80,** 1923.

Tanimoto, T., 1987. Surface-wave ray tracing equations and Fermat's principle in an anisotropic Earth, *Geophys. J. R. astr. Soc.,* **88,** 231–240.

Tanimoto, T. & Anderson, D.L., 1984. Mapping convection in the mantle, *Geophys. Res. Lett.,* **11,** 287–290.

Tanimoto, T. & Anderson, D.L., 1985. Lateral heterogeneity and azimuthal anisotropy of the upper mantle: Love and Rayleigh waves 100–250 s, *J. geophys. Res.,* **90,** 1842–1858.

Tape, C.H., 2003. Waves on a spherical membrane, *MSc thesis,* Oxford University, Oxford, UK.

Trampert, J. & Woodhouse, J.H., 2003. Global anisotropic phase velocity maps for fundamental mode surface waves between 40 and 150 s, *Geophys. J. Int.,* **154,** 154–165.

Trefethen, L.N. & Bau, D., III, 1997. *Numerical Linear Algebra*, Soc. for Ind. and Appl. Math., Philadelphia, Pennsylvania, USA.

Wessel, P. & Smith, W.H.F., 1991. Free software helps map and display data, *EOS, Trans. Am. geophys. Un.,* **72,** 445–446.

Woodhouse, J.H. & Wong, Y.K., 1986. Amplitude, phase and path anomalies of mantle waves, *Geophys. J. R. astr. Soc.,* **87,** 753–773.

APPENDIX A: ALGORITHM FOR THE CALCULATION OF GENERALIZED SPHERICAL HARMONICS AND ROTATION MATRICES

The generalized spherical harmonics $Y_{lm}^N(\theta, \phi)$ (Phinney & Burridge 1973) are:

$$Y_{lm}^N(\theta, \phi) = e^{im\phi} P_l^{Nm}(\cos\theta), \tag{A1}$$

where

$$P_l^{Nm}(\mu) = 2^{-l}(-1)^{l-N}\sqrt{\frac{(l+m)!}{(l+N)!(l-N)!(l-m)!}} \times$$
$$\times (1-\mu)^{-(m-N)/2}(1+\mu)^{-(m+N)/2}\left(\frac{d}{d\mu}\right)^{l-m}[(1-\mu)^{l-N}(1+\mu)^{l+N}]. \tag{A2}$$

Equivalently,

$$Y_{lm}^N(\theta, \phi) = e^{im\phi} d_{Nm}^{(l)}(\theta), \tag{A3}$$

where $d_{Nm}^{(l)}(\theta) = P_l^{Nm}(\cos\theta)$ are the rotation matrix elements employed in the quantum mechanical theory of angular momentum (Edmonds 1960). Regarded as matrices in which N is a row index ($-l \leq N \leq l$) and m is a column index ($-l \leq m \leq l$), $d_{Nm}^{(l)}(\theta)$ are the representations of rotation group elements corresponding to rotation by θ about the y-axis of the standard coordinate system, in the $(2l+1)$-dimensional representation of the rotation group (see Edmonds 1960). Hence the algorithm described here can also be used to generate the rotation matrices needed to rotate spherical harmonic coefficients and generalized spherical harmonic coefficients from one set of axes to another. If the coordinate system is changed by a rotation having Euler angles α, β, γ (Edmonds 1960)the matrix multiplying the vector of expansion coefficients is given by

$$\mathcal{D}_{m'm}^{(l)}(\alpha, \beta, \gamma) = e^{im'\gamma} d_{m'm}^{(l)}(\beta) e^{im\alpha}. \tag{A4}$$

This matrix acts on a (column) vector of harmonic coefficients ($-l \leq m \leq l$) for each given value of l.

A formula equivalent to (A.2) is:

$$d_{Nm}^{(l)}(\theta) = \sqrt{\frac{(l-N)!\,(l+N)!}{(l-m)!\,(l+m)!}} (\cos\theta/2)^{N+m} (\sin\theta/2)^{N-m} P_{l-N}^{(N-m,\,N+m)}(\cos\theta) \tag{A5}$$

where $P_n^{(\alpha,\beta)}(\mu)$ are the Jacobi polynomials.

The algorithm we use to calculate $d_{Nm}^{(l)}(\theta)$ makes use of the following recurrence relation:

$$\sqrt{(l-m)(l+m+1)}\,d_{Nm}^{(l)}(\theta) = -2\,[(m+1)\cot\theta - N\csc\theta]\,d_{Nm+1}^{(l)}(\theta)$$
$$- \sqrt{(l-m-1)(l+m+2)}\,d_{Nm+2}^{(l)}(\theta), \tag{A6}$$

together with the special case:

$$d_{Nl}^{(l)}(\theta) = (-1)^{l-N}\sqrt{\frac{(2l)!}{(l-N)!\,(l+N)!}} (\cos\theta/2)^{l+N} (\sin\theta/2)^{l-N}. \tag{A7}$$

For a given value of l, eq. (A.7) defines the values in the rightmost column ($m = l$) of the $(2l+1) \times (2l+1)$ matrix and the recurrence (A6) is used to step down in column number (i.e. to the left along each row), to generate the entries in the row. In the first step use is made of the fact that $d_{Nl+1}^{(l)}(\theta) = 0$ (the entries to the right of the rightmost column can be taken to be zero) and thus the second term on the right side of (A6) is absent. In practise, the values in the rightmost column are initially set to 1, and then each row is subsequently rescaled by the value given by (A7). This allows the algorithm to give correct results in cases where, for example, θ is very small, in which case the off-diagonal elements of the matrix are also very small and the diagonal elements are close to 1. To avoid numerical overflow and underflow in such cases an exponent for each element is stored in the initially unused (see below) left side of the matrix and when the values become very small during rescaling that element is set to 0. It is necessary to iterate towards the diagonals to avoid numerical instabilities, particularly for high values of l. Thus the recurrence along each row N is continued only as far as the element for which $|m| = |N|$. The part of the $(2l+1) \times (2l+1)$ matrix thus filled is the triangle above the leading diagonal and below the subdiagonal. After the rescaling of the rows, the remainder of the matrix is filled using the formulae:

$$d_{mN}^{(l)}(\theta) = (-1)^{N-m} d_{Nm}^{(l)}(\theta) = d_{-N-m}^{(l)}(\theta), \tag{A8}$$

which relate elements through reflection in the diagonal and the subdiagonal.

In practise, the entries in the rightmost column are also generated by a recurrence relation starting at the top-right corner ($N = -N_{max}$, $m = l$), again making use of separately stored exponents to avoid potential numerical underflow and overflow. The necessary recurrence relation follows easily from (A6).

An advantage of the strategy employed by this algorithm over other potential strategies is that the matrix needs to be generated only for the values of N which are of interest in a given application; only the rows of the matrix corresponding to $-N_{max} \leq N \leq N_{max}$ are calculated. The middle row of the matrix, which is the only row if $N_{max} = 0$, contains the scalar spherical harmonics $Y_{lm}^0(\theta, 0)$, ($-l \leq m \leq l$). In this study, when it is required to trace rays through a given anisotropic model, we need $N_{max} = 4$. To express the expansion coefficients of anisotropic phase velocity in a rotated coordinate system, on the other hand, the full matrix is needed—that is, $N_{max} = l$.

A computer program implementing this algorithm can be obtained from the authors on request.

We do not claim that this algorithm is optimally efficient. If the application requires only small values of N_{max} it may be advantageous to make use of explicit representations of $d^{(l)}_{Nm}(\theta)$ in terms of $d^{(l)}_{0m}(\theta)$ (essentially the associated Legendre functions, used for the calculation of scalar spherical harmonics) and its derivative with respect to θ. In the present application a more efficient scheme for ray tracing may be to evaluate the contravariant components of phase velocity (in the sense of Phinney & Burridge 1973) on a grid capturing the ray, for example, a latitude–longitude grid in the coordinate system in which the source and the receiver are on the 'equator'. Such grids can be generated very efficiently as it is necessary to evaluate $d^{(l)}_{Nm}(\theta)$ only once for each value of θ that defines the grid.

See also Masters & Richards-Dinger (1998).